

# Core-Softened System With Attraction: Trajectory Dependence of Anomalous Behavior

Yu. D. Fomin and E. N. Tsiok

*Institute for High Pressure Physics, Russian Academy of Sciences, Troitsk 142190, Moscow Region, Russia*

V. N. Ryzhov

*Institute for High Pressure Physics, Russian Academy of Sciences, Troitsk 142190, Moscow Region, Russia and Moscow Institute of Physics and Technology, Dolgoprudnii, Moscow region, Russia*

(Dated: May 25, 2021)

In the present article we carry out a molecular dynamics study of the core-softened system and show that the existence of the water-like anomalies in this system depends on the trajectory in  $P - \rho - T$  space along which the behavior of the system is studied. For example, diffusion and structural anomalies are visible along isotherms as a function of density, but disappears along the isochores and isobars as a function of temperature. On the other hand, the diffusion anomaly may be seen along adiabats as a function of temperature, density and pressure. It should be noted that it may be no signature of a particular anomaly along a particular trajectory, but the anomalous region for that particular anomaly can be defined when all possible trajectories in the same space are examined (for example, signature of diffusion anomaly is evident through the crossing of different isochors. However, there is no signature of diffusion anomaly along a particular isochor). We also analyze the applicability of the Rosenfeld entropy scaling relations to this system in the regions with the water-like anomalies. It is shown that the validity of the Rosenfeld scaling relation for the diffusion coefficient also depends on the trajectory in the  $P - \rho - T$  space along which the kinetic coefficients and the excess entropy are calculated.

PACS numbers: 61.20.Gy, 61.20.Ne, 64.60.Kw

## I. INTRODUCTION

It is well known that some liquids (for example, water, silica, silicon, carbon, phosphorus, and some biological systems) show an anomalous behavior in the vicinity of their freezing lines [1–21]. The water phase diagrams have regions where a thermal expansion coefficient is negative (density anomaly), self-diffusivity increases upon compression (diffusion anomaly), and the structural order of the system decreases with increasing pressure (structural anomaly) [6, 7].

The first anomaly mentioned above is density anomaly. It means that density increases upon heating or that the thermal expansion coefficient becomes negative. Using the thermodynamic relation  $(\partial P/\partial T)_V = \alpha_P/K_T$ , where  $\alpha_P$  is a thermal expansion coefficient and  $K_T$  is the isothermal compressibility and taking into account that  $K_T$  is always positive and finite for systems in equilibrium not at a critical point, we conclude that density anomaly corresponds to minimum of the pressure dependence on temperature along an isochor. This is the most convenient indicator of density anomaly in computer simulation.

If we consider a simple liquid (for, example, Lennard-Jones liquid), and trace the diffusion along an isotherm we find that the diffusion decreases under densification. This observation is intuitively clear - if density increases the free volume decreases and the particles have less freedom to move. However, some substances have a region in density - temperature plane where diffusion grows under

densification. This is called anomalous diffusion region which reflects the contradiction of this behavior with the free volume picture described above. This means that diffusion anomaly involves more complex mechanisms which will be discussed below.

The last anomaly we discuss here is structural anomaly. Initially this anomaly was introduced via order parameters characterizing the local order in liquid. However, later on the local order was also related to excess entropy of the liquid which is defined as the difference between the entropy and the ideal gas entropy at the same  $(\rho, T)$  point:  $S_{ex} = S - S_{id}$ . In normal liquid excess entropy is monotonically decaying function of density along an isotherm while in anomalous liquids it demonstrates increasing in some region. This allows to define the boundaries of structural anomaly at given temperature as minimum and maximum of excess entropy.

The regions where these anomalies take place form nested domains in the density-temperature [6] (or pressure-temperature [7]) planes: the density anomaly region is inside the diffusion anomaly domain, and both of these anomalous regions are inside a broader structurally anomalous region. It is reasonable to relate this kind of behavior to the orientational anisotropy of the potentials, however, a number of studies demonstrate water-like anomalies in fluids that interact through spherically symmetric potentials [22–52].

As it was discussed in many works (see, for example, the reviews [22] and [47]) the presence of two length scales in the core-softening potential may be the origin of water-

like anomalies: a larger one, associated with the external finite repulsion (effective at lower pressures and temperatures), and a smaller one, related to the particle hard core (dominant at higher pressures and temperatures). In those thermodynamic regimes where the two length scales are both partially effective and thus are competing with each other, a system of particles interacting through such potentials behaves, in many respects, as a mixture of two species of different sizes. This leads to the existence of two competing local structures: an expanded structure characterized by large open spaces between particles, and a collapsed structure in which particles are spaced more closely. The evolution of these structures under changing the thermodynamic conditions can result in the anomalous behavior. For example, as it was shown in many works (see, for example, [54]), the low temperature thermodynamic anomalies of liquid water arises from the intermittent fluctuation between its high density and low density forms, consisting largely of 5-coordinated and 4-coordinated water molecules, respectively.

However, it should be noted that in general the existence of two length scales is not enough to mark the occurrence of the anomalies. For example, for the models studied in Ref. [55] it was shown that the existence of two distinct repulsive length scales is not a necessary condition for the occurrence of anomalous phase behavior.

The problem of anomalous behavior of core-softened fluids was widely discussed in literature (see, for example, the recent review [22]). It was shown that for some systems the anomalies take place while for others do not [22]. In this respect the question of criteria of anomalous behavior appearance remains the central one. However, another important point is still lacking in the literature - the behavior of anomalies along different thermodynamic trajectories. Here we call as "trajectory" a set of points belonging to some path in  $(P, \rho, T)$  space. For example, the set of points belonging to the same isotherm we call as "isothermal trajectory" or shortly isotherm.

In our previous work we showed [56, 57] that anomalies can exist along some trajectories while along others the liquid behaves as a simple one. Taking into account this result, it is interesting to study the behavior of the quantities demonstrating anomalies along the different physically significant trajectories (isotherms, isochors, isobars and adiabats). This investigation will allow to get deeper understanding of the relations between anomalous behavior and thermodynamic parameters of the system which spread light on the connection between thermodynamic, structural and dynamic properties of liquids.

## II. SYSTEM AND METHODS

The simplest form of core-softened potential is the so called Repulsive Step Potential which is defined as fol-

lowing:

$$U(r) = \begin{cases} \infty, & r \leq d \\ \varepsilon, & d < r \leq \sigma \\ 0, & r > \sigma \end{cases} \quad (1)$$

where  $d$  is the diameter of the hard core,  $\sigma$  is the width of the repulsive step, and  $\varepsilon$  is its height. In the low-temperature limit  $\tilde{T} \equiv k_B T / \varepsilon \ll 1$  the system reduces to a hard-sphere system with hard-sphere diameter  $\sigma$ , whilst in the limit  $\tilde{T} \gg 1$  the system reduces to a hard-sphere model with a hard-sphere diameter  $d$ . For this reason, melting at high and low temperatures follows simply from the hard-sphere melting curve  $P = cT/\sigma'^3$ , where  $c \approx 12$  and  $\sigma'$  is the relevant hard-sphere diameter ( $\sigma$  and  $d$ , respectively). A changeover from the low- $T$  to high- $T$  melting behavior should occur for  $\tilde{T} = \mathcal{O}(1)$ . The precise form of the phase diagram depends on the ratio  $s \equiv \sigma/d$ . For large enough values of  $s$  one should expect to observe in the resulting melting curve a maximum that should disappear as  $s \rightarrow 1$ . The phase behavior in the crossover region may be very complex, as shown in [48, 52].

In the present simulations we have used a smoothed version of the repulsive step potential (Eq. (1)), which has the form:

$$U(r) = \varepsilon \left( \frac{d}{r} \right)^n + \frac{1}{2} \varepsilon (1 - \tanh(k_0 (r - \sigma_s))), \quad (2)$$

where  $n = 14, k_0 = 10$ . We have considered  $\sigma_s = 1.35$ . Here and below we refer to this potential as to Smooth Repulsive Shoulder System (SRSS).

In the remainder of this paper we use the dimensionless quantities:  $\tilde{\mathbf{r}} \equiv \mathbf{r}/d$ ,  $\tilde{P} \equiv Pd^3/\varepsilon$ ,  $\tilde{V} \equiv V/Nd^3 \equiv 1/\tilde{\rho}$ . As we will only use these reduced variables, we omit the tildes.

In Refs. [48, 52], phase diagrams of SRSS models were reported for  $\sigma_s = 1.15, 1.35, 1.55, 1.8$ .

Fig. 1 shows the phase diagrams that we obtain from the free-energy calculations for  $\sigma_s = 1.35$ . In fact, the phase diagrams for  $\sigma_s = 1.15, 1.35, 1.55, 1.8$  were already reported in Refs. [48, 52]. We show these phase diagrams here too because they provide the "landscape" in which possible "water" anomalies should be positioned.

Fig. 1(a) shows the phase diagram of the system with  $\sigma_s = 1.35$  in the  $\rho - T$  plane. There is a clear maximum in the melting curve at low densities. The phase diagram consists of two isostructural FCC domains corresponding to close packing of the small and large spheres separated by a sequence of structural phase transitions. This phase diagram was discussed in detail in our previous publications [48, 52]. It is important to note that there is a region of the phase diagram where we have not found any stable crystal phase. The results of Ref. [48] suggest that a glass transition occurs in this region with vitrification temperature  $T_g = 0.079$  at  $\rho = 0.53$ . The apparent glass-transition temperature is above the melting point of the

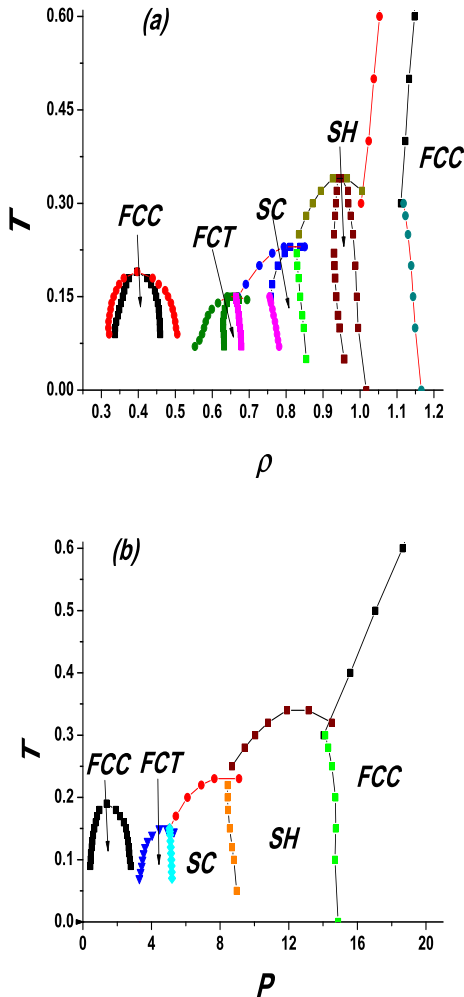


FIG. 1: (Color online). Phase diagram of the system of particles interacting through the potential (2) with  $\sigma_s = 1.35$  in  $\rho - T$  (a) and  $P - T$  (b) planes.

low-density FCC and FCT phases. If, indeed, no other crystalline phases are stable in this region, the “glassy” phase that we observe would be thermodynamically stable. This is rather unusual for one-component liquids. In simulations, glassy behavior is usually observed in metastable mixtures, where crystal nucleation is kinetically suppressed. One could argue that, in the glassy region, the present system behaves like a “quasi-binary” mixture of spheres with diameters  $d$  and  $\sigma_s$  and that the freezing-point depression is analogous to that expected in a binary system with an eutectic point: there are some values of the diameter ratio such that crystalline structures are strongly unfavorable and the glass phase could then be stable even at very low temperatures. The glassy behavior in the reentrant liquid disappears at higher temperatures.

In the present study a system of particles interacting

via the potential with “hard” core, repulsive shoulder and attractive well is also investigated. This potential represents a generalization of our previous SRSS model [48, 52] and we call it Smooth Repulsive Shoulder System with Attractive Well (SRSS-AW) potential [53].

The general form of the potential is written as

$$U(r) = \varepsilon \left(\frac{\sigma}{r}\right)^{14} + \varepsilon (\lambda_0 - \lambda_1 \tanh(k_1\{r - \sigma_1\}) + \lambda_2 \tanh(k_2\{r - \sigma_2\})). \quad (3)$$

We consider only the potentials with  $\sigma_1 = 1.35$  (see Table 1).

Before to proceed, let us consider the analytic condition for core softening proposed in Ref. [58]:

$$rU''(r) + U'(r) < 0, r_2 > r > r_1 \quad (4)$$

and also

$$U''(r) > 0 \quad (5)$$

for  $r < r_1$  and  $r > r_2$ , where  $r_1$  and  $r_2$  denote two repulsive length scales. In the systems satisfying these conditions there are two local structures which compete with each other. In this case the system behaves as the mixture of two types of particles with effective radii  $r_1$  and  $r_2$  (see, for example, Ref. [48]), and one can expect to find a reentering melting and other anomalous behaviors.

It may be easily seen that for the potentials (1-3) (see Table 1) the conditions (4) and (5) are satisfied for  $\sigma_1 \geq 1.16$ , so in the case  $\sigma_1 = 1.35$  the anomalies do exist [52, 53].

However, as it was mentioned above, in general the conditions (4) and (5) are not enough to mark the occurrence of the anomalies [55].

In Refs. [22, 23] the extensive study of the softness dependence of the anomalies for the continuous shouldered well potential was presented and different criteria for the appearance of the anomalies was analyzed. It was shown that for the more steeper soft-core the regions of the density and diffusion anomalies become more narrow, while the region of the structural anomaly is only weakly affected, and the disappearance of the density and diffusion anomalies for the steeper potentials is due to a more structured short-range order. At the same time, it may be shown that the conditions (4) and (5) are satisfied for the potentials considered in Refs. [22, 23]. For the steeper potentials the range between  $r_1$  and  $r_2$  is more narrow, and the effective diameter of the soft core is larger. However, as it was shown earlier [52], the increasing of the soft core diameter leads to the disappearance of the anomalies in the range of the thermodynamic stability of the system. It seems that the search of the adequate criterium relating the appearance of the anomalies with the intermolecular potential is very interesting and important problem.

number	$\sigma_1$	$\sigma_2$	$\lambda_0$	$\lambda_1$	$\lambda_2$	well depth
1	1.35	0	0.5	0.5	0	0
2	1.35	1.80	0.5	0.60	0.10	0.20
3	1.35	1.80	0.5	0.7	0.20	0.4

TABLE I: The potential parameters used in simulations (Eq. (3)).

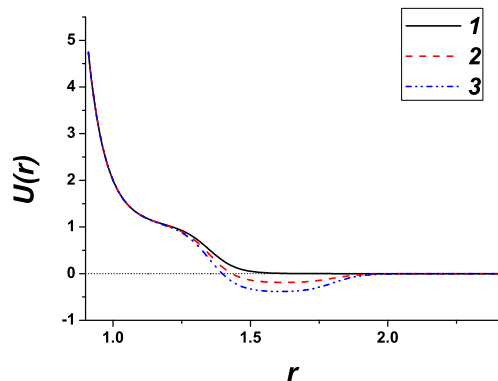


FIG. 2: (Color online) Family of the potentials with  $\sigma_1 = 1.35$  and different attractive wells. The curves are numerated in accordance with Table 1.

We consider the system with the step  $\sigma_1 = 1.35$ . The parameters  $k_1 = k_2 = 10.0$  are fixed while parameters  $\sigma_2, \lambda_0, \lambda_1$  and  $\lambda_2$  are varied to get the different potential shape. Three sets of parameters are considered. They are summarized in Table 1. Fig. 2 shows the potentials for the step width  $\sigma_1 = 1.35$  respectively. The parameters are chosen in such a way that the depth of attractive well becomes larger (see Table 1 and Fig. 2). Below we denote the systems with different parameters as system 1, system 2 and so on in accordance with the Table 1. The choice of the potential parameters was dictated only by the convenience for the analysis of the qualitative influence of the attraction on the properties of the system.

In our previous publications [48, 52] we discussed the phase diagrams of several purely repulsive systems, i.e. the systems with zero well depth. The complexity of these phase diagrams was shown. The systems with attractive well were considered in [53]. For the completeness we present the evolution of the system behavior with increasing attraction in Figs. 3 and 4.

The transition lines were determined from the free energy calculations [59, 60].

We simulate the system in  $NVT$  ensemble using Monte-Carlo method. The number of particles in the liquid or gas state simulation was set to 500 or 1000 and for crystal phases it varied between 500 and 1000 depending on the structure. The system was equilibrated for  $10^6$  MC step and the data were collected during  $10^5$  MC steps.

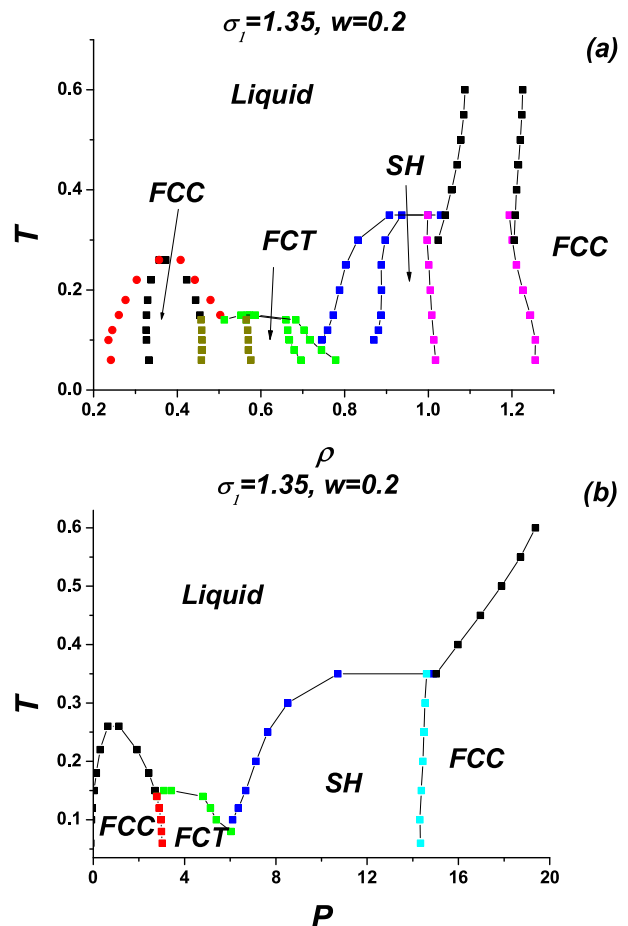


FIG. 3: (Color online) Phase diagram of the system 2 (Table 1) in (a)  $\rho - T$  and (b)  $P - T$  coordinates.

In order to find the transition points we carry out the free energy calculations for different phases and construct a common tangent to them. For the purely repulsive potentials we computed the free energy of the liquid by integrating the equation of state along an isotherm [59, 60]:  $\frac{F(\rho) - F_{id}(\rho)}{Nk_B T} = \frac{1}{k_B T} \int_0^\rho \frac{P(\rho') - \rho' k_B T}{\rho'^2} d\rho'$ . In the case of potentials which contain an attractive part the situation is more complicated because of the possible gas - liquid transition. In order to avoid the difficulties connected to this transition we carry out calculation of free energies at high temperature above the gas - liquid critical point and then calculate the free energies by integrating the internal energies along an isochor [59, 60]:  $\frac{F(T_2) - F(T_1)}{k_B T} = \int_{T_1}^{T_2} U(T, N, V) d(\frac{1}{T})$ .

Free energies of different crystal phases were determined by the method of coupling to the Einstein crystal [59, 60].

To improve the statistics (and to check for internal consistency) the free energy of the solid was computed at many dozens of different state points and fitted to multinomial function. The fitting function we used is  $a_{p,q} T^p V^q$ , where  $T$  and  $V = 1/\rho$  are the temperature and

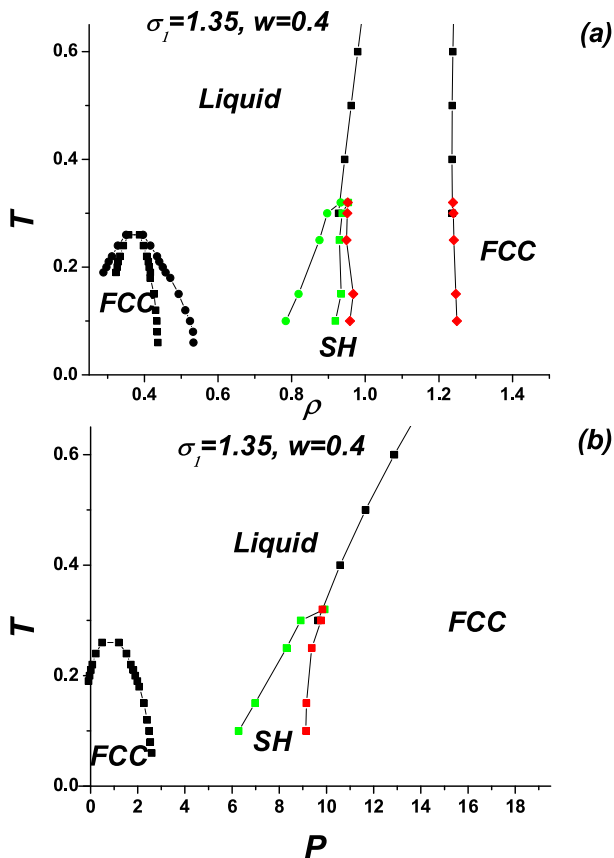


FIG. 4: (Color online) Phase diagram of the system 3 (Table 1) in (a)  $\rho - T$  and (b)  $P - T$  coordinates.

specific volume and powers  $p$  and  $q$  are related through  $p + q \leq N$ . The value  $N$  we used for the most of calculations is 5.

The diffusion anomaly is also discussed in the article. Since the diffusion coefficient can not be measured in Monte Carlo simulations, molecular dynamics is applied. The core-softened systems are characterized by a complex energy landscape. This makes difficult to simulate the system at low temperatures. In order to avoid this problem, parallel tempering technique is used [59, 60]. The diffusion is measured along a set of isochors between the densities  $\rho = 0.3$  and  $\rho = 0.8$ . The temperatures used are confined between  $T = 0.15$  and  $T = 0.8$ .

We simulate a system of 864 particles in a cubic box. Each parallel tempering run consists of 16 exchanges between 8 different temperatures. Between the exchanges the system evolves for  $4 \cdot 10^6$  steps. The first  $3 \cdot 10^6$  steps are used for equilibration. The time step is  $dt = 0.0005$ . In order to keep the temperature constant Andersen thermostat is used during the equilibration. Summing up all simulations done and taking into account exchange of temperatures in parallel tempering runs, we collect more than a hundred measurements along each isochor which gives good statistics. The diffusion coefficient

along isochors is approximated by a 9–th order polynomial of temperature. Then the data are rearranged along isotherms.

### III. RESULTS AND DISCUSSION

#### Diffusion anomaly

The diffusion anomaly of the SRSS was discussed in several our previous articles. In the Refs. [48, 52, 53] we showed that the diffusion anomaly takes place at the shoulder width  $\sigma_1 = 1.35$  while in the work [65] the breakdown of the Rosenfeld scaling for this system was demonstrated. Further discussion of the Rosenfeld scaling was reported in the works [56, 57]. The main idea of these papers is that the anomalous diffusion behavior present along low-temperature isotherms while along isochors diffusion coefficient is monotonous. As a result, Rosenfeld scaling is valid along isochors and high-temperature isotherms, however, it breaks down for the isotherms with anomalies. It means that appearance or not of anomalies at some trajectory can cause physically different behavior of the system. As a result, following different trajectories, we can or can not observe some effects. It is of particular importance since experimental works deal mostly with isobars and isotherms while theoretical studies - with isochors and isotherms. Taking this into account, one can expect that some of the effects observed along isobars are not visible along isotherms and isochors which makes us confused while comparing experimental results with theoretical predictions. Here we extend the study of anomalies to four different physically meaningful trajectories: isotherms, isochors, isobars and adiabats and consider both SRSS and SRSS-AW potentials.

Fig. 5(a) shows the diffusion coefficient of SRSS system along a set of isotherms for  $\sigma_1 = 1.35$  (potential 1 in Table 1). One can see that the diffusion coefficient demonstrates anomalous behavior for the temperatures below  $T = 0.25$ . On the other hand, if we look at the Fig. 5(b) where the same diffusion coefficient data are arranged along isochors as a function of temperature we do not observe anomalies - the diffusion is a monotonous function of temperature along isochors. However, some of the isochors cross. One can see, that the cross of the isochors corresponds to the densities between  $\rho = 0.4$  and  $\rho = 0.6$ . Comparing it to the isotherms we see that this is the region of anomalous diffusion. It means that even if we do not see nonmonotonous behavior of diffusion along isochors we can identify the presence of anomaly from crossing of the isochors. However, this method seems to be technically more difficult since we need to measure many points belonging to different isochors rather than one isotherm. In Fig. 5(c) the diffusion coefficient is shown as a function of pressure along the isochores.

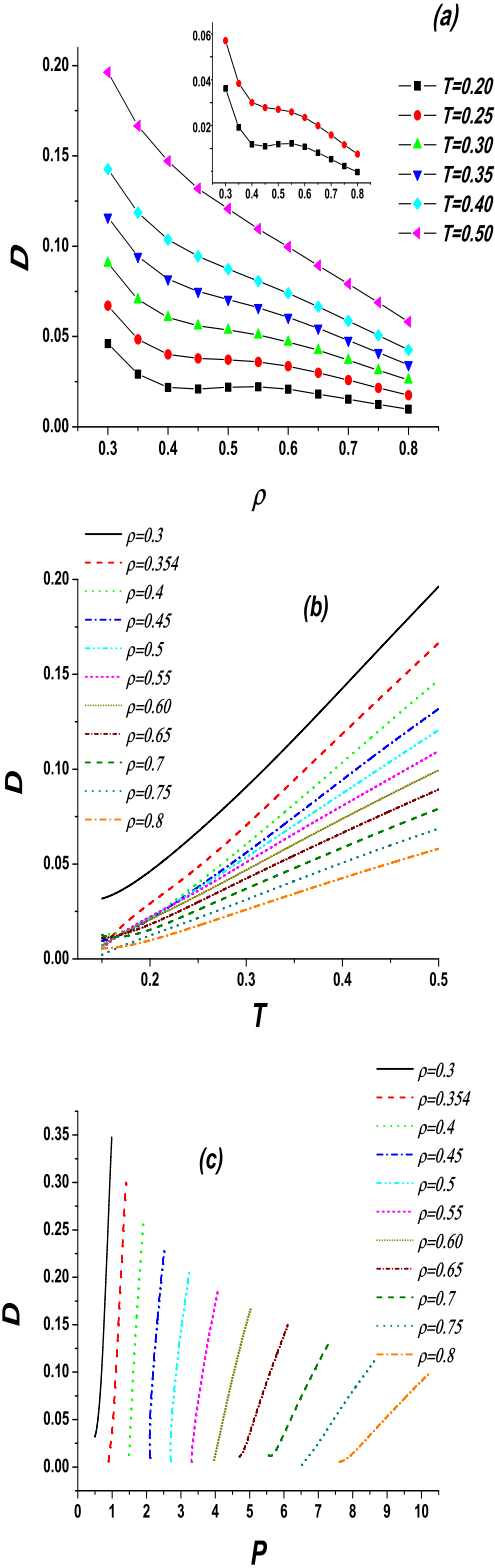


FIG. 5: (Color online). Diffusion coefficient of the SRSS system along (a) isotherms and (b) and (c) - isochors. The insert in (a) shows the low temperature isotherms.

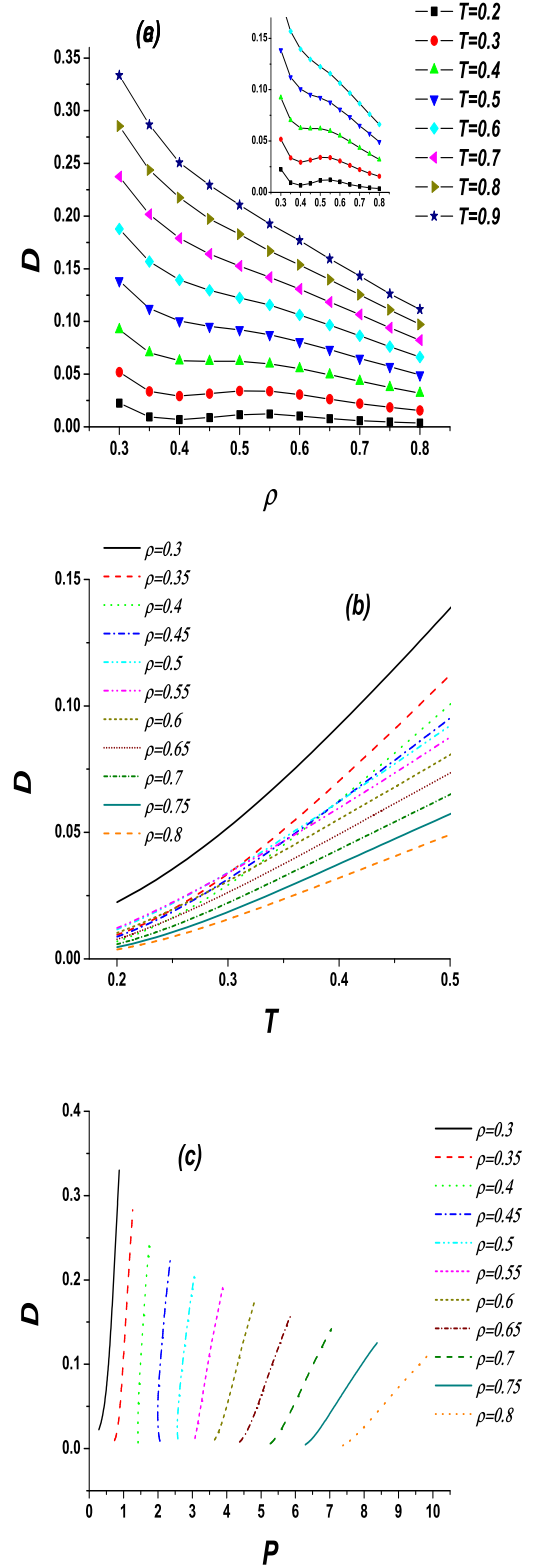


FIG. 6: (Color online). Diffusion coefficient of the SRSS-AW system (system 3 in Table 1) along (a) isotherms and (b) and (c) - isochors.

One can see that in the range of the densities between  $\rho = 0.4$  and  $\rho = 0.6$  the slopes of the curves change sign. Isothermal and isochoric behavior of diffusion in anomalous region for SRSS have already been discussed in our previous publications [56, 57] and we give these plots here for the sake of completeness.

If attraction is added to the potential (systems 2 and 3 in Table 1), no new qualitative features are found, however, the anomalies become more pronounced. One can see this, for example, in Figs. 6 ((a), (b) and (c)), where the diffusion coefficients of the SRSS-AW potential of the system 3 are shown along the isotherms and isochores.

Fig. 7(a) shows the diffusion coefficient along a set of isobars as a function of density. The diffusion coefficient is again monotonous. The slope of the curves is always negative. However, as it can be seen from the insert, the slope approaches infinity at low diffusions at pressures  $P = 2.0$  and  $P = 2.5$ . This corresponds to densities  $0.45 - 0.50$  inside the anomalous region. One can imagine that if we lower the temperatures along these isobars we can observe change of the slope to positive one, however, we do not have data for these temperatures.

Fig. 7(b) shows the diffusion coefficient along isobars as a function of temperature. The situation is analogous to the case of isochores: the curves are monotonous, however, they intersect at low temperatures, corresponding to anomalous region (see the insert in Fig. 7(b)). It means that if we have the diffusion coefficient along isobars we can identify the presence of anomalies by monitoring the intersections of the curves. However, by the reasons discussed above this method is not practically convenient.

Figs. 8((a) and (b)) show the diffusion coefficient along isobars as functions of density and temperature if attraction is added (system 3 in Table 1). As in the case of isotherms and isochores, the attraction makes the anomalies more pronounced. For example, without attraction we could find only hints of the diffusion anomaly as a function of density (Fig. 7 (a)), however, this anomaly is explicit for the system 3 (see Fig. 8 (a)).

The last physically meaningful trajectory considered in the present work is the adiabat. This trajectory is defined as constant entropy curve. The entropy is calculated as following. We compute excess free energy by integrating the equation of states:  $\frac{F_{ex}}{Nk_B T} = \frac{F - F_{id}}{Nk_B T} = \frac{1}{k_B T} \int_0^\rho \frac{P(\rho') - \rho' k_B T}{\rho'^2} d\rho'$ . The excess entropy can be computed via  $S_{ex} = \frac{U - F_{ex}}{Nk_B T}$ . The total entropy is  $S = S_{ex} + S_{id}$ , where the ideal gas entropy is  $\frac{S_{id}}{Nk_B} = \frac{3}{2} \ln(T) - \ln(\rho) + \ln\left(\frac{(2\pi m k_B)^{3/2} e^{5/2}}{h^3}\right)$ . The last term in this expression is constant and is not accounted in our calculations.

The behavior of entropy itself will be discussed below. Here we give the diffusion coefficients along the adiabats (Fig. 9 (a)-(c)).

One can see from the Fig. 9 (a)-(c) that the anomaly

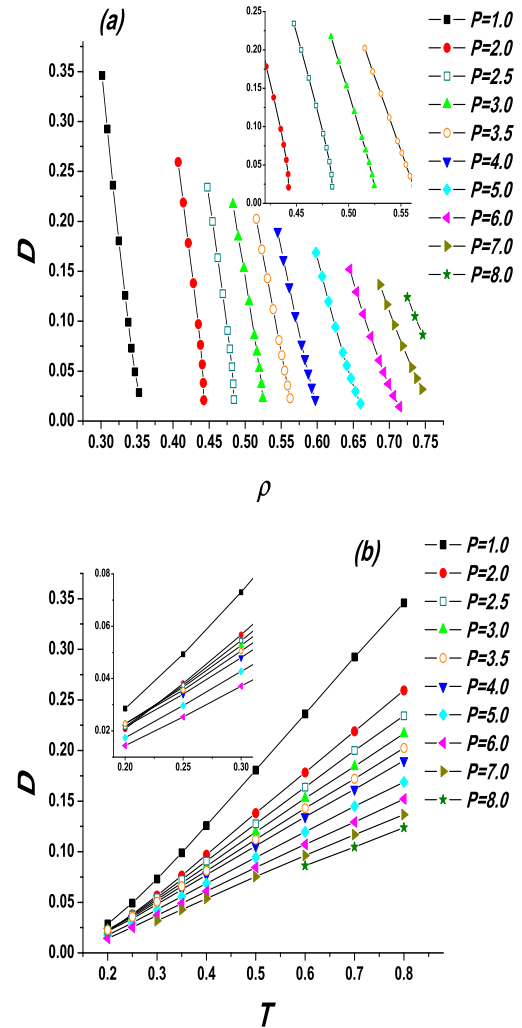


FIG. 7: (Color online). Diffusion coefficient of the SRSS system along isobars as a function of (a) density and (b) temperature. The inserts show anomalous regions in the corresponding coordinates.

takes place along adiabats in all possible coordinates (look, for example,  $S = -4.0$  adiabat). It means that in case of adiabatic trajectory one can identify the anomalous region monitoring any of three thermodynamic variables ( $P, \rho, T$ ). However, this trajectory is rather difficult to realize in simulation or experiment.

As one can expect, the attraction does not produce qualitative changes in the behavior of the anomalies, but makes them more explicit. We do not show the corresponding figures.

### Density Anomaly

As we mentioned above density anomaly corresponds to appearance of a minima on isochores of the system. The

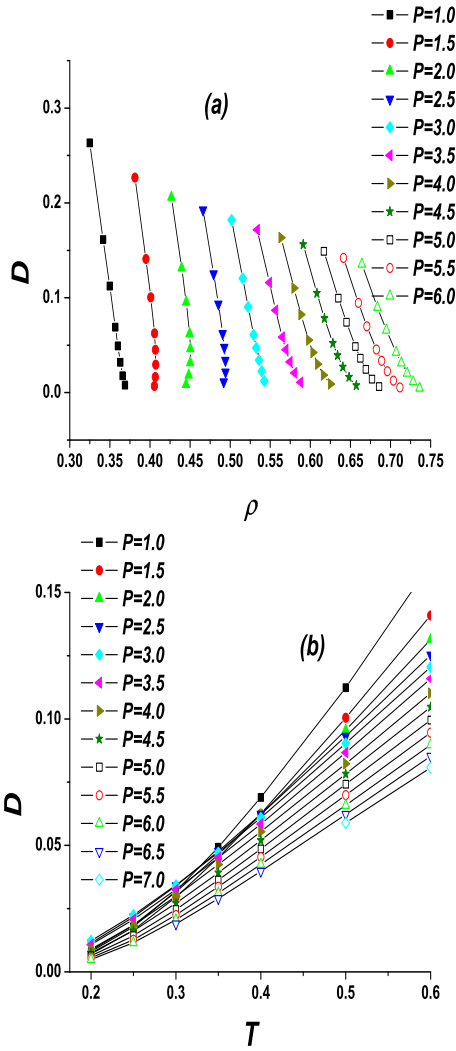


FIG. 8: (Color online). Diffusion coefficient of the SRSS-AW system (system 3 in Table 1) along isobars as a function of (a) density and (b) temperature.

isochors of the system with the potential (2) (system 1 in Table 1) are shown in the Fig. 10(a). It is evident from the figure that some of the isochors do demonstrate minima. The location of the minimum in the  $\rho - T$  plane is shown in Fig. 10(b).

If we turn to the shape of the isobars themselves for the potential (2) (system 1 in Table 1), that is the dependence of temperature on density at fixed pressure, we do not find any traces of anomalies there (Fig. 11). Like in the case of diffusion, the curves have negative slope which approaches zero at low temperatures and densities corresponding to anomalous regime. However, the curve remains monotonous, and it seems that there is no sign of density anomaly along isobars. However, using the well known thermodynamic relation:

$$\left(\frac{\partial V}{\partial T}\right)_P \left(\frac{\partial T}{\partial P}\right)_V \left(\frac{\partial P}{\partial V}\right)_T = -1, \quad (6)$$

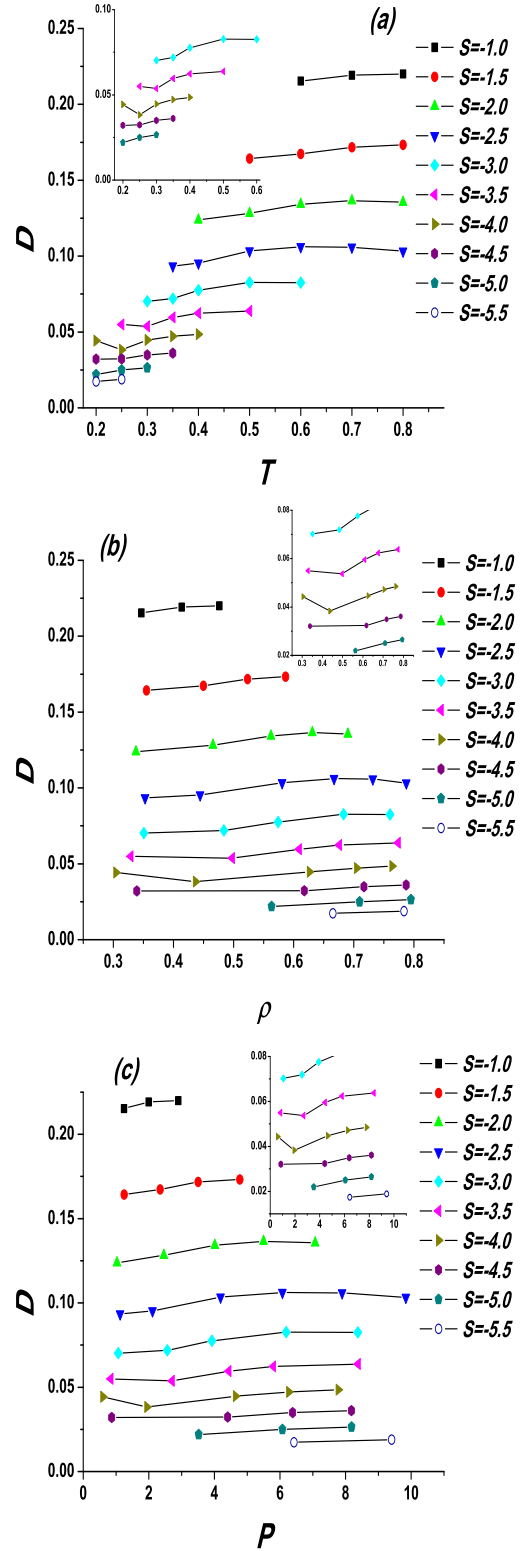


FIG. 9: (Color online). Diffusion coefficient of the SRSS system along adiabats as a function of (a) temperature, (b) density, and (c) pressure. The inserts show anomalous regions in the corresponding coordinates.

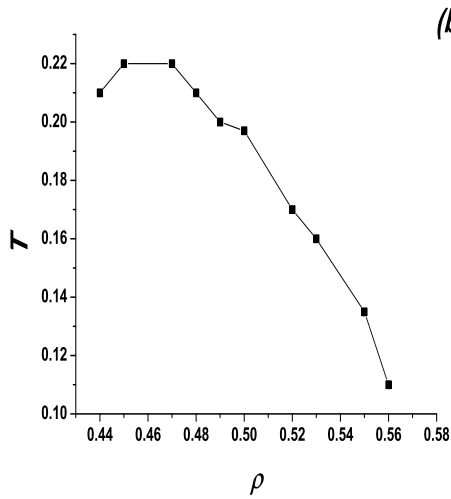
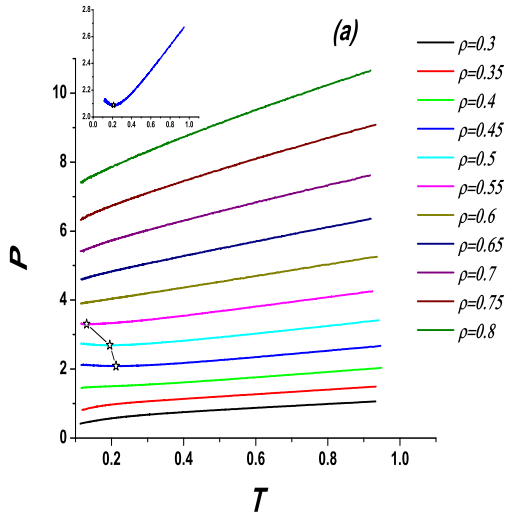


FIG. 10: (Color online). (a) A set of isochors of SRSS. The stars show the location of minimum. The insert enlarges the  $\rho = 0.45$  isochor. (b) The location of the minima on isochors in  $\rho - T$  plane.

one can find that  $K_T \left( \frac{\partial P}{\partial T} \right)_V \left( \frac{\partial T}{\partial \rho} \right)_P = -\frac{N}{\rho^2}$ , where  $K_T$  is the isothermal compressibility. Taking into account that  $K_T$  is always positive and finite for systems in equilibrium, and using Fig. 10(a), one can see that  $\left( \frac{\partial T}{\partial \rho} \right)_P > 0$  if  $\left( \frac{\partial P}{\partial T} \right)_V < 0$ . We can conclude that the anomaly does exist along isobars for low temperatures, but we do not see it in our simulations.

As it was mentioned above, adding the attraction to the potential makes the anomalies more pronounced. To illustrate this, in Fig. 12 we show the isobars for the system 3 (see Table 1) where the anomalies are clear seen.

Figs. 13 ((a) and (b)) show adiabats of the SRSS in  $\rho - T$  and  $P - T$  coordinates. Interestingly, the curves seem monotonic, but the slope of the curves at low and high densities (pressures) is very different. At the same

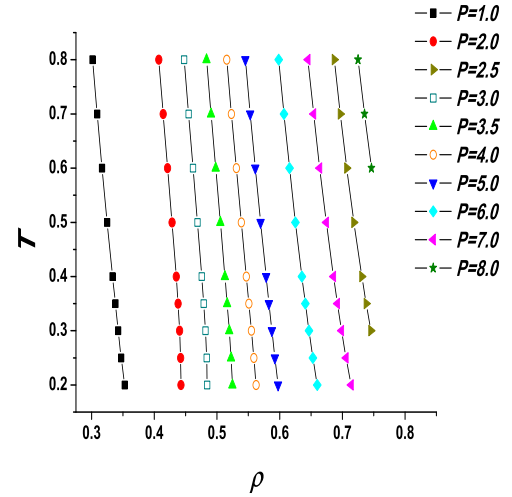


FIG. 11: (Color online). A set of isobars of SRSS.

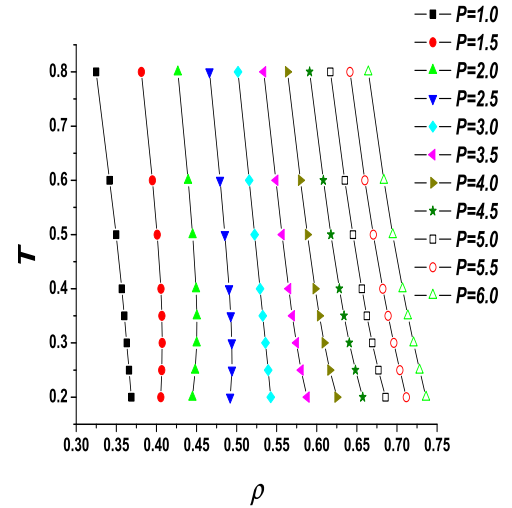


FIG. 12: (Color online). A set of isobars of SRSS-AW (system 3 in Table 1).

time the middle density (pressure) curves demonstrate a continues change from the high slope (low-density regime) to low slope (high-density regime). However, from the well-known thermodynamic relation  $\left( \frac{\partial T}{\partial \rho} \right)_S = \rho^2 \frac{T}{c_v} \left( \frac{\partial P}{\partial T} \right)_V$  and Fig. 10 one can see that in the case of Fig. 13 (a) the anomaly does exists, but it is not seen because of the insufficient accuracy of calculations along the adiabats. On the other hand, due to the relation  $\left( \frac{\partial T}{\partial P} \right)_S = \frac{T}{c_P} \left( \frac{\partial V}{\partial T} \right)_P$  there is also anomalous behavior in Fig. 13 (b).

As one can expect (we do not represent these figures here for the sake of brevity), the anomalies are much better seen for the systems with the attractive potentials (systems 2 and 3 in Table 1).

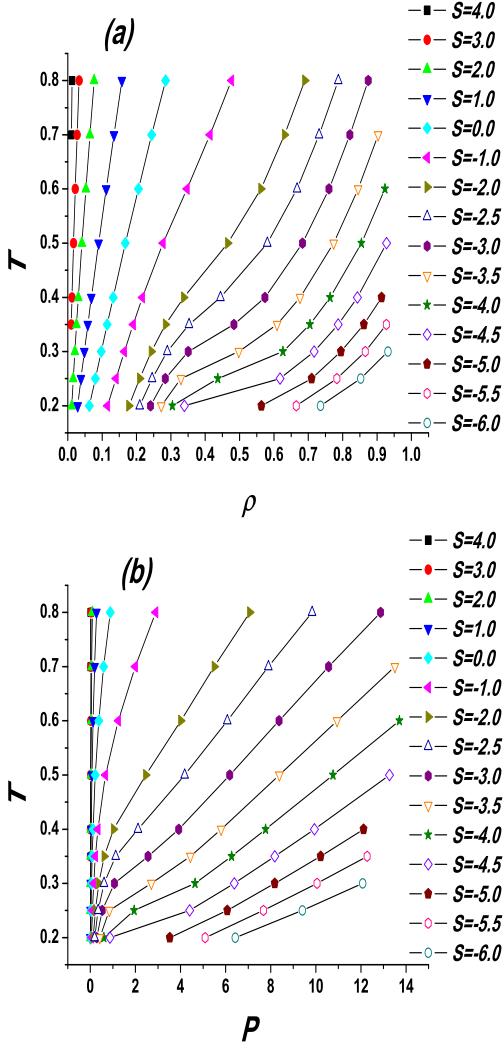


FIG. 13: (Color online). Adiabats of the SRSS in (a)  $\rho - T$  and (b)  $P - T$  coordinates.

### Structural Anomaly

Structural anomaly region can be bounded by using the local order parameters or by excess entropy minimum and maximum. Here we apply the definition via excess entropy.

The behavior of excess entropy is qualitatively analogous to the behavior of diffusion coefficient. Because of this we briefly describe it here noting that most of the conclusions about diffusion coefficient along different trajectories can be applied to excess entropy as well.

Figs. 14 ((a) and (b)) show the excess entropy along isotherms and isochors for the purely repulsive potential (2). Like for the diffusion coefficient, excess entropy demonstrates anomalous growth in some density range at low temperatures. At the same time excess entropy is monotonous along isochors. However, the curves for different isochors cross which indicates the presence of

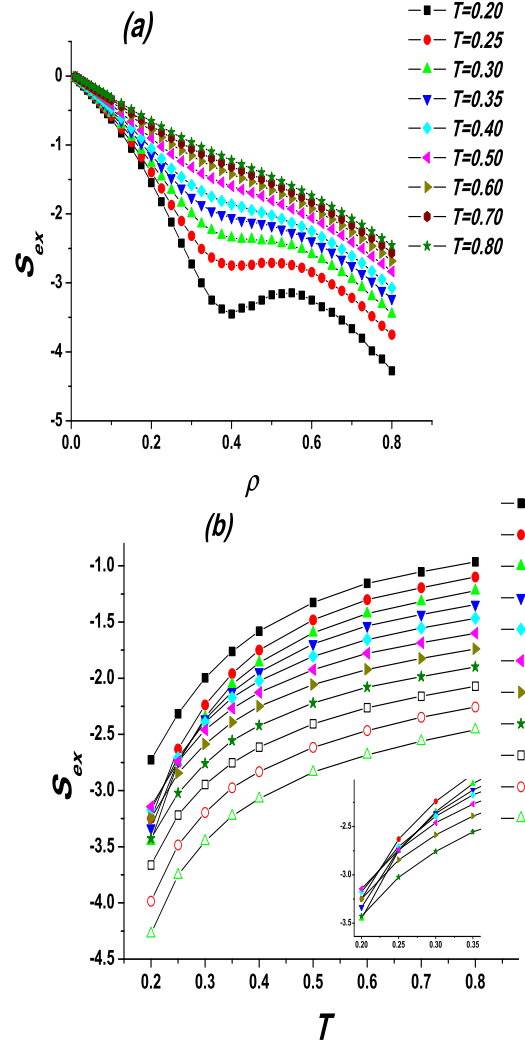


FIG. 14: (Color online). Excess entropy of SRSS fluid along (a) isotherms and (b) isochors.

anomaly.

The excess entropy along isobars is monotonically decreasing function of density and monotonically increasing function of temperature (see Figs. 15((a) and (b))). However, the curves cross at low temperatures indicating the presence of anomalies as it was discussed for the case of diffusion. As in the case of diffusion anomaly, the structural anomaly is not seen along the isobars for the purely repulsive potential (system 1 in Table 1), however, one can expect that in our simulation we could not reach the anomalous region. If the attraction is added to the potential, the anomaly becomes explicit even as a function of density (see Figs. 16((a) and (b))).

It is important to note that the range of densities of structural anomalies is wider than the one of diffusion and density anomalies which is consistent with the literature data for core-softened systems [6, 7]. Figs. 17((a), (b) and (c)) represent the locations of the anomalies lines on

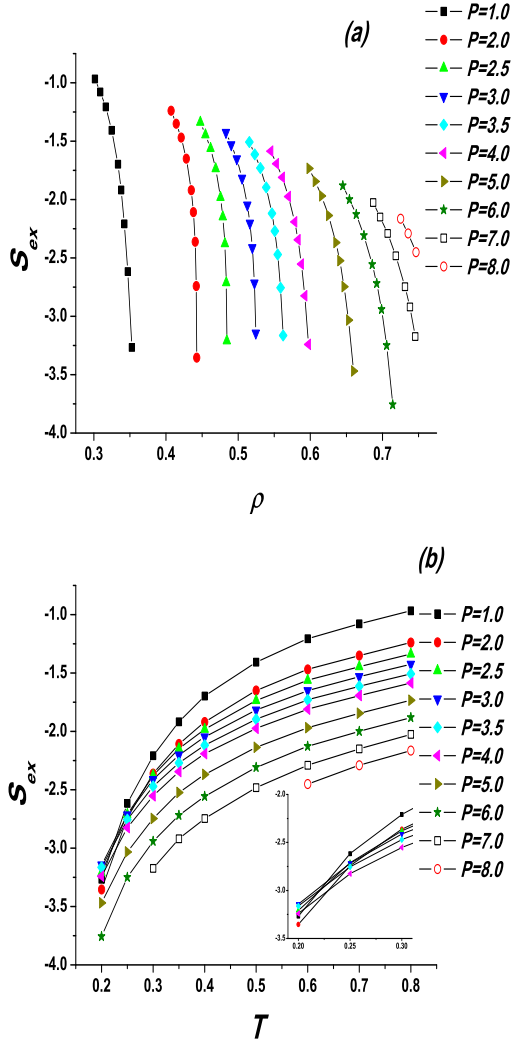


FIG. 15: (Color online). Excess entropy of SRSS fluid along isobars as a function of (a) density and (b) temperature. The insert in (b) shows the cross of the curves at low temperatures.

the phase diagrams of the systems in Table 1 in  $\rho - T$  plane.

#### IV. ROSENFELD SCALING

In 1977 Rosenfeld proposed a connection between thermodynamic and dynamical properties of liquids [61, 62]. The main Rosenfeld's statement claims that the transport coefficients are exponential functions of the excess entropy. In order to write the exponential relations Rosenfeld introduced reduction of the transport coefficients by some macroscopic parameters of the system. For the case of diffusion coefficient one writes:  $D^* = D \frac{\rho^{1/3}}{(k_B T/m)^{1/2}}$ , where  $m$  is the mass of the particles. The Rosenfeld scaling rule can be written as:

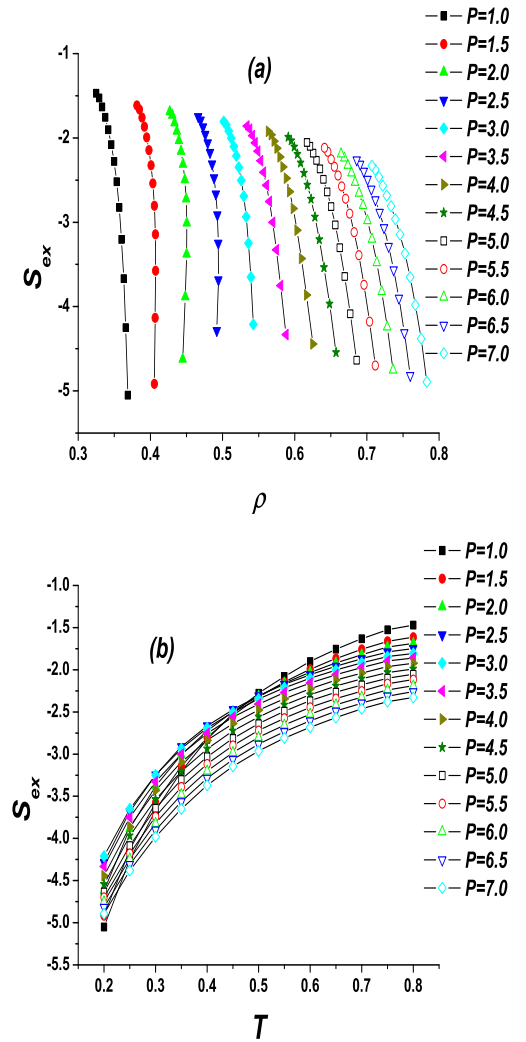


FIG. 16: (Color online). Excess entropy of SRSS-AW fluid along isobars as a function of (a) density and (b) temperature (system 3 in Table 1).

$$D^* = A \cdot e^{BS_{ex}}, \quad (7)$$

where  $A$  and  $B$  are constants.

In his original works Rosenfeld considered hard spheres, soft spheres, Lennard-Jones system and one-component plasma [61, 62]. After that the excess entropy scaling was applied to many different systems including core-softened liquids [18, 19, 63–65], liquid metals [66, 67], binary mixtures [68, 69], ionic liquids [70, 71], network-forming liquids [63, 70], water [72], chain fluids [73] and bounded potentials [65, 74, 75].

In our recent publication [56, 57, 65] we showed that for the case of the core-softened fluids the applicability of Rosenfeld relation depends on the trajectory. In particular, Rosenfeld relation is applicable along isochors, but it is not applicable along isotherms.

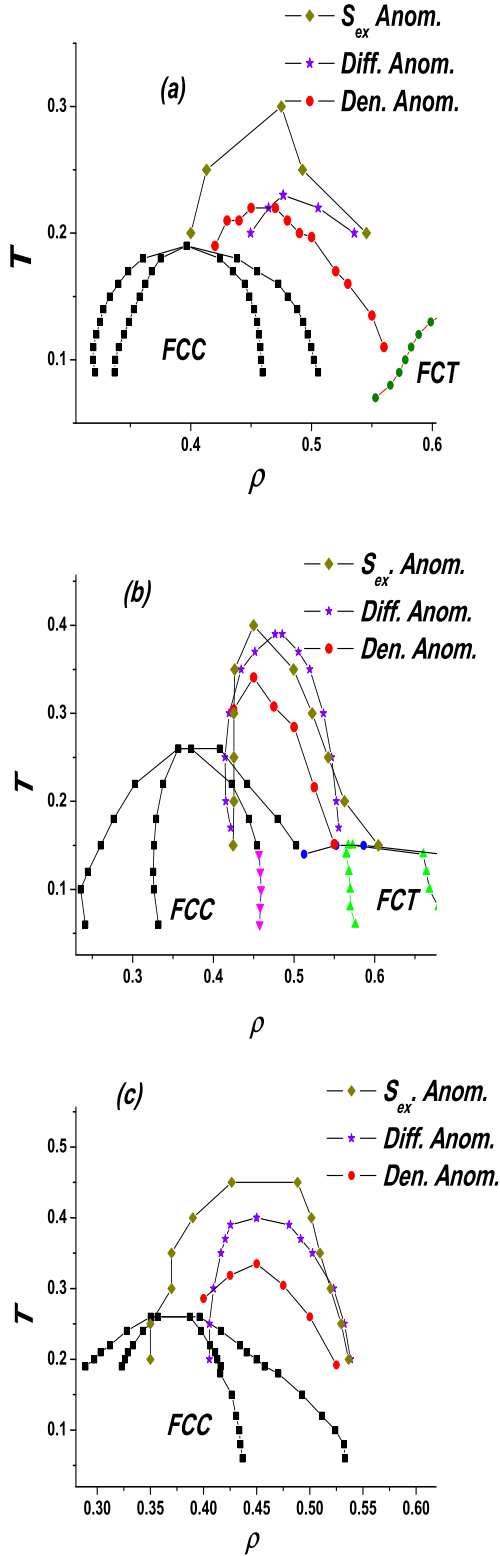


FIG. 17: (Color online). Locations of the anomalies lines on the phase diagrams in  $T-\rho$  plane for the system 1 (a), system (2) (b), and System 3 (c) from Table 1.

The breakdown of the Rosenfeld relation along isotherms can be seen from the following speculation. The regions of different anomalies do not coincide with each other. In particular, in the case of core-softened fluids the diffusion anomaly region is located inside the structural anomaly one. It means that there are some regions where the diffusion is still normal while the excess entropy is already anomalous. But this kind of behavior can not be consistent with the Rosenfeld scaling law.

However, from this speculation it follows that the Rosenfeld scaling should hold true along the trajectories which do not contain anomalies, i.e. isochors and isobars. In our recent publication [57] we considered the Rosenfeld relation along isotherms and isochors. Here we bring these trajectories for the sake of completeness and add the verification of the Rosenfeld relation along isobars for the purely repulsive potential (2) (Figs. 18(a) - (c)). One can see that the Rosenfeld relation does break down along isotherms which is consistent with the speculation above. At the same time it holds true along both isochors and isobars which is consistent with the monotonous behavior of both diffusion coefficient and excess entropy along these trajectories.

In Figs. 19((a) - (c)) we show the Rosenfeld relation for the system 3. One can see that the behavior is the same as in the case of the purely repulsive potential.

This observation makes evident that Rosenfeld relation is valid only along the trajectories without anomalous behavior.

## V. SUMMARY AND DISCUSSION

To summarize, in the present article we carry out a molecular dynamics study of the core-softened systems (SRSS and SRSS-AW) and show that the anomalous behavior can be seen only along some particular trajectories in  $(P, \rho, T)$  space along which the behavior of the system is studied. For example, diffusion and structural anomalies are visible along isotherms as a function of density, but disappears along the isochores and isobars as a function of temperature. On the other hand, the diffusion anomaly may be seen along adiabats as a function of temperature, density and pressure. Density anomaly exists along isochors, isobars and adiabats. However, if a single curve does not demonstrate the anomalous behavior, having a set of the curves, one can see the presence of anomalies via the curves crossing.

We also analyze the applicability of the Rosenfeld entropy scaling relations to this system in the regions with the water-like anomalies. It is shown that the validity of the Rosenfeld scaling relation for the diffusion coefficient also depends on the trajectory in the  $P-\rho-T$  space along which the kinetic coefficients and the excess entropy are calculated. In particular, it is valid along isochors and isobars, but it breaks down along isotherms. The break-

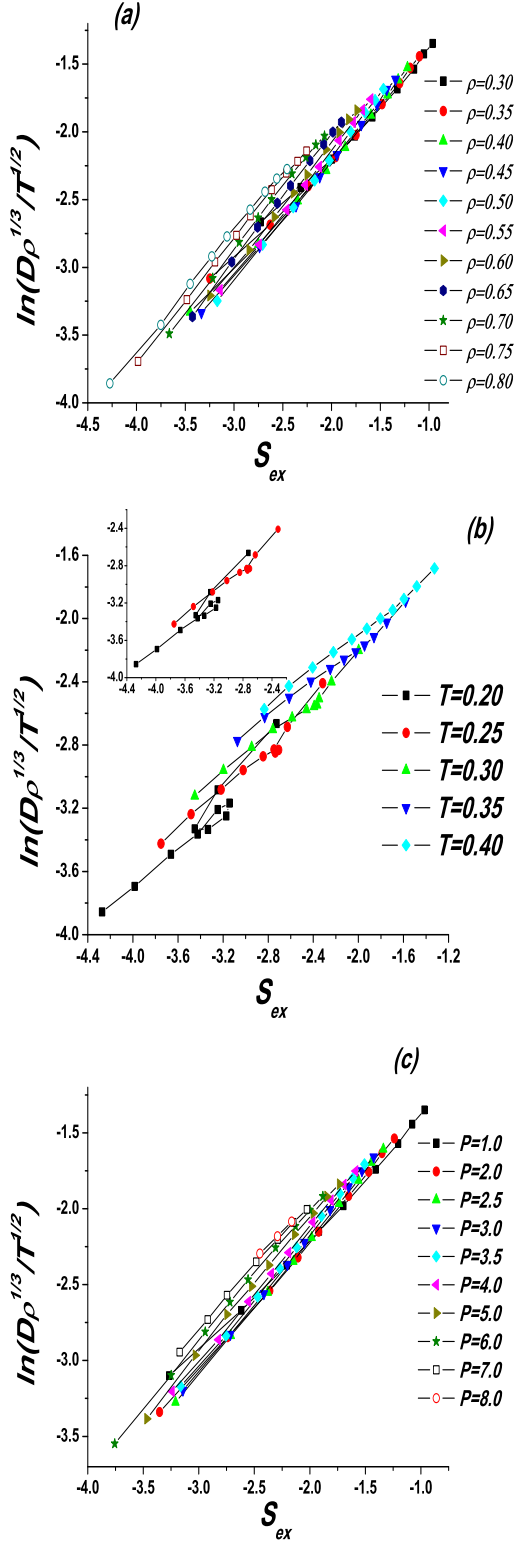


FIG. 18: (Color online). Rosenfeld relation for SRSS along (a) isochors, (b) isotherms, and (c) isobars.

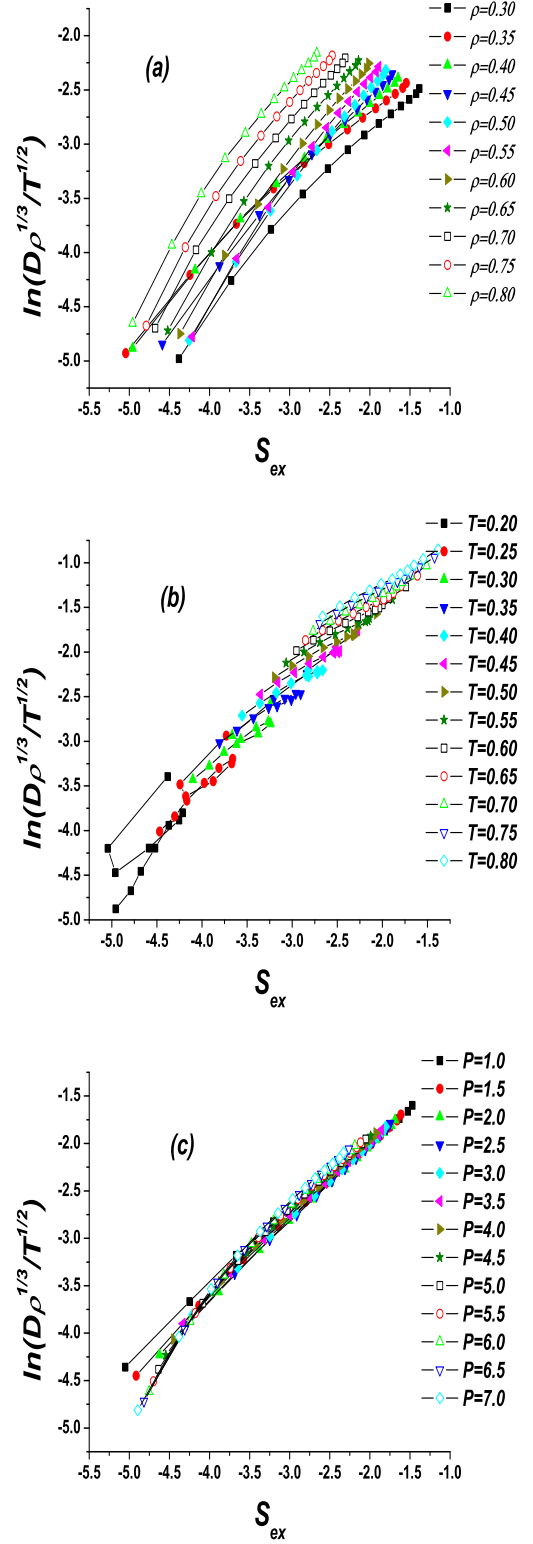


FIG. 19: (Color online). Rosenfeld relation for SRSS-AW along (a) isochors, (b) isotherms, and (c) isobars.

down of the Rosenfeld relation along isotherms is related to the fact that the boundaries of different anomalies do not coincide with each other.

The influence of attraction on the diffusion anomaly is discussed. It is shown that the attraction makes the anomalies much more clear and may be found even in the cases when the anomalies are hardly seen for the purely repulsive potential due to simulation limitations.

The question is whether this type of behavior is universal for all types of systems demonstrating the anomalous behavior. It is now widely believed that the water anomalies are related with the hypothesized liquid-liquid critical point, the terminal point of a line of first-order liquid-liquid phase transitions [8, 9, 76–78]. The anomalies arise from crossing the Widom line emanating from the hypothesized liquid-liquid critical point (LLCP) [77–79]. In particular, it was shown [77] that the dynamical crossover from Arrhenius to non-Arrhenius behavior (strong-fragile transition) takes place both for water and Jagla [33] model. The Jagla model with attraction displays (without the need to supercool) a liquid-liquid coexistence line that, unlike water, has a positive slope [77]. We believe that our model should show the similar phase behavior as the Jagla one, however, with the LLCP in the deeply supercooled region [53].

For example, in Figs. 20 ((a) - (c)) we show the behavior of the isothermal compressibility  $K_T$ , the isobaric heat capacity  $C_P$ , and the thermal expansion coefficient  $\alpha_P$  for the system 1 in Table 1. One can see that the system demonstrates the behavior compatible with hypothesis of the liquid-liquid critical point in the deep supercooled region of the phase diagram below the homogeneous nucleation line (compare, for example, with Fig. 1 in Ref. [79]). In Fig. 21 one can see the dynamical crossover from Arrhenius to non-Arrhenius behavior. At high temperature,  $D$  exhibits an Arrhenius behavior, whereas at low temperature it follows a non-Arrhenius one. From Figs. 20 and 21 one can easily see that the anomalous lines correspond to the regions of anomalies in Fig. 1 (b). This result is consistent with the case of the Jagla model [77] (see Fig. 5 (c) in Ref. [77]), so we believe that in our case the Widom line should have the same slope, as in this model, and we can expect that the anomalous behavior discussed in this article will be the same for the Jagla model too, however, the case of water needs an additional investigation.

We thank V. V. Brazhkin for stimulating discussions. Y.F. and E.T. also thank Russian Scientific Center Kurchatov Institute and Joint Supercomputing Center of Russian Academy of Science for computational facilities. The work was supported in part by the Russian Foundation for Basic Research (Grants No 10-02-00694a, 10-02-00700 and 11-02-00-341a) and Russian Federal Programs 02.740.11.5160 and 02.740.11.0432.

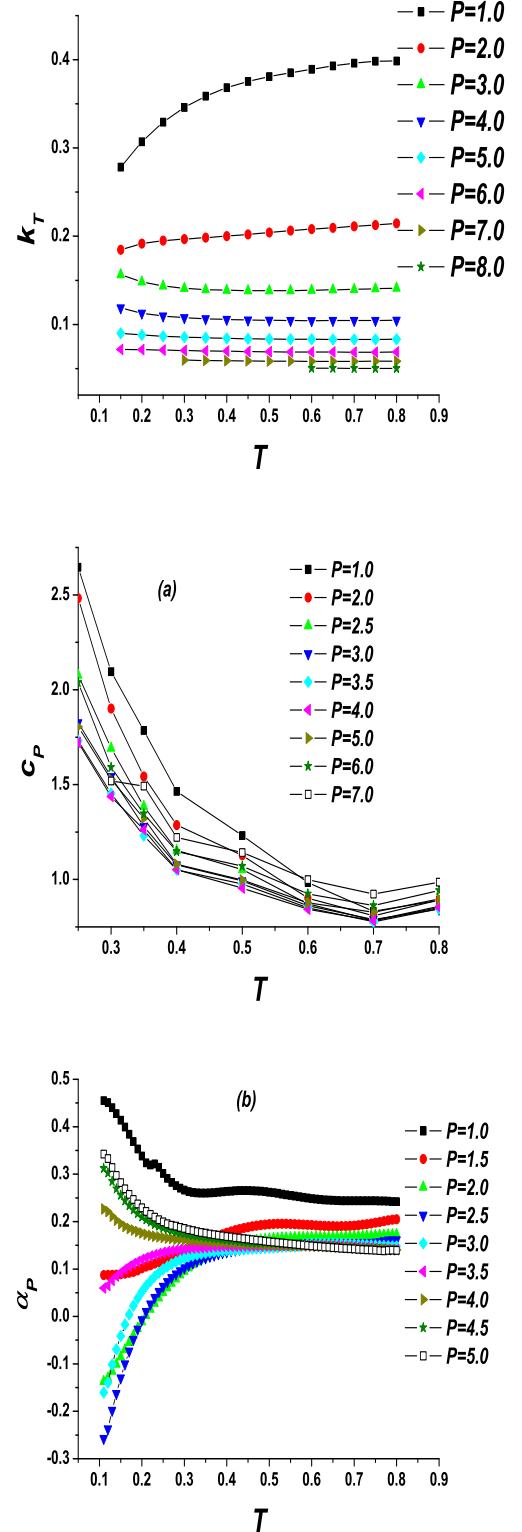


FIG. 20: (Color online). Isothermal compressibility  $K_T$  (a), isobaric heat capacity  $C_P$  (b), and thermal expansion coefficient  $\alpha_P$  (c) as a function of temperature along isobars for the system 1 in Table 1.

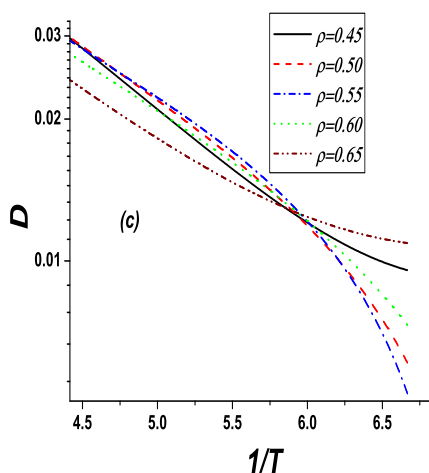


FIG. 21: (Color online). Diffusivity  $D$  along isochores for the system 1 in Table 1.

- [1] P. Debenedetti, J. Phys.: Condens. Matter **15**, R1669 (2003).
- [2] S. V. Buldyrev, G. Franzese, N. Giovambattista, G. Malescio, M. R. Sadr-Lahijany, A. Scala, A. Skibinsky, and H. E. Stanley, Physica A **304**, 23 (2002).
- [3] C. A. Angell, Annu. Rev. Phys. Chem. **55**, 559 (2004).
- [4] P. G. Debenedetti, *Metastable Liquids: Concepts and Principles* (Princeton University Press, Princeton, 1998).
- [5] V. V. Brazhkin, S. V. Buldyrev, V. N. Ryzhov, and H. E. Stanley [eds], *New Kinds of Phase Transitions: Transformations in Disordered Substances* [Proc. NATO Advanced Research Workshop, Volga River] (Kluwer, Dordrecht, 2002).
- [6] J. R. Errington and P. G. Debenedetti, Nature (London) **409**, 18 (2001).
- [7] P.A. Netz, F.V. Starr, H.E. Stanley, and M.C. Barbosa, J. Chem. Phys. **115**, 318 (2001).
- [8] O. Mishima and H. E. Stanley, Nature **396**, 329 (1998).
- [9] Franzese, G. Malescio, A. Skibinsky, S.V. Buldyrev, and H. E. Stanley, Nature **409**, 692 (2001).
- [10] C.A. Angell, E.D. Finch, and P. Bach, J. Chem. Phys. **65**, 3063 (1976).
- [11] H. Thurn and J. Ruska, J. Non-Cryst. Solids **22**, 331 (1976).
- [12] G.E. Sauer and L.B. Borst, Science **158**, 1567 (1967).
- [13] F.X. Prielmeier, E.W. Lang, R.J. Speedy, H.-D. Lüdemann, Phys. Rev. Lett. **59**, 1128 (1987).
- [14] F.X. Prielmeier, E.W. Lang, R.J. Speedy, H.-D. Lüdemann, B. Bunsenges, Phys. Chem. **92**, 1111 (1988).
- [15] L. Haar, J. S. Gallagher, G. S. Kell, NBS/NRC Steam Tables. Thermodynamic and Transport Properties and Computer Programs for Vapor and Liquid States of Water in SI Units, Hemisphere Publishing Co., Washington DC, 1984, pp. 271-276.
- [16] A. Scala, F. W. Starr, E. LaNave, F. Sciortino and H. E. Stanley, Nature **406**, 166 (2000).
- [17] <http://www.lsbu.ac.uk/water/anmlies.html>
- [18] J. R. Errington, Th. M. Truskett, J. Mittal, J. Chem. Phys. **125**, 244502 (2006).
- [19] J. Mittal, J. R. Errington, Th. M. Truskett J. Chem. Phys. **125**, 076102 (2006).
- [20] P. Kumar, L. Xu, Z. Yan, M. G. Mazza, S. V. Buldyrev, S. H. Chen, S. Sastry, and H. E. Stanley, Phys. Rev. Lett., **97**, 177802 (2006).
- [21] D. Biswal, B. Jana, S. Pal, and B. Bagchi, J. Phys. Chem. B **113**, 4394 (2009).
- [22] Pol Vilaseca and Giancarlo Franzese, Journal of Non-Crystalline Solids **357**, 419 (2011).
- [23] Pol Vilaseca and Giancarlo Franzese, J. Chem. Phys., **133**, 084507 (2010).
- [24] P. C. Hemmer and G. Stell, Phys. Rev. Lett. **24**, 1284(1970).
- [25] G. Stell and P. C. Hemmer, J. Chem. Phys. **56**, 4274 (1972).
- [26] G. Malescio, J. Phys.: Condens. Matter **19**, 07310 (2007).
- [27] E. Velasco, L. Mederos, G. Navascues, P. C. Hemmer, and G. Stell, Phys. Rev. Lett. **85**, 122 (2000).
- [28] P. C. Hemmer, E. Velasco, L. Mederos, G. Navascues, and G. Stell, J. Chem. Phys. **114**, 2268 (2001).
- [29] M. R. Sadr-Lahijany, A. Scala, S. V. Buldyrev and H. E. Stanley, Phys. Rev. Lett. **81**, 4895 (1998).
- [30] M. R. Sadr-Lahijany, A. Scala, S. V. Buldyrev and H. E. Stanley, Phys. Rev. E **60**, 6714 (1999).
- [31] P. Kumar, S. V. Buldyrev, F. Sciortino, E. Zaccarelli, and H. E. Stanley, Phys. Rev. E **72**, 021501 (2005).
- [32] L. Xu, S. V. Buldyrev, C. A. Angell, and H. E. Stanley, Phys. Rev. E **74**, 031108 (2006).
- [33] E. A. Jagla, J. Chem. Phys. **111**, 8980 (1999); E. A. Jagla, Phys. Rev. E **63**, 061501 (2001).
- [34] F. H. Stillinger and D. K. Stillinger, Physica (Amsterdam) **244A**, 358 (1997).
- [35] A. B. de Oliveira, P. A. Netz, T. Colla, and M. C. Barbosa, J. Chem. Phys. **124**, 084505 (2006).
- [36] A. B. de Oliveira, P. A. Netz, T. Colla, and M. C. Barbosa, J. Chem. Phys. **125**, 124503 (2006).
- [37] P. A. Netz, S. Buldyrev, M. C. Barbosa and H. E. Stanley, Phys. Rev. E **73**, 061504 (2006).
- [38] A. B. de Oliveira, M. C. Barbosa, and P. A. Netz, Physica A **386**, 744 (2007).
- [39] J. Mittal, J. R. Errington, and T. M. Truskett, J. Chem. Phys. **125**, 076102 (2006).
- [40] H. M. Gibson and N. B. Wilding, Phys. Rev. E **73**, 061507 (2006).
- [41] P. Camp, Phys. Rev. E **71**, 031507 (2005).
- [42] A. B. de Oliveira, G. Franzese, P. A. Netz, and M. C. Barbosa, J. Chem. Phys. **128**, 064901 (2008).
- [43] L. Xu, S. Buldyrev, C. A. Angell, and H. E. Stanley, Phys. Rev. E **74**, 031108 (2006).
- [44] A. B. de Oliveira, P. A. Netz, and M. C. Barbosa, Euro. Phys. J. B **64**, 481 (2008).
- [45] A. B. de Oliveira, P. A. Netz, and M. C. Barbosa, arXiv:0804.2287v1.
- [46] Z. Yan, S. V. Buldyrev, N. Giovambattista, and H. E. Stanley, Phys. Rev. Lett. **95**, 130604 (2005).
- [47] S. V. Buldyrev, G. Malescio, C. A. Angell, N. Giovambattista, S. Prestipino, F. Saija, H. E. Stanley and L. Xu, J. Phys.: Condens. Matter **21**, 504106 (2009).
- [48] Yu. D. Fomin, N. V. Gribova, V. N. Ryzhov, S. M. Stishov, and Daan Frenkel, J. Chem. Phys. **129**, 064512 (2008).
- [49] V. N. Ryzhov and S. M. Stishov, Zh. Eksp. Teor. Fiz.

- 122**, 820 (2002)[JETP **95**, 710 (2002)].
- [50] V. N. Ryzhov and S. M. Stishov, Phys. Rev. E **67**, 010201(R) (2003).
- [51] Yu. D. Fomin, V. N. Ryzhov, and E. E. Tareyeva, Phys. Rev. E **74**, 041201 (2006).
- [52] N. V. Gribova, Yu. D. Fomin, Daan Frenkel, V. N. Ryzhov, Phys. Rev. E **79**, 051202 (2009).
- [53] Yu. D. Fomin, V. N. Ryzhov, and E. N. Tsiok, J. Chem. Phys. **134**, 044523 (2011).
- [54] B. Jana, and B. Bagchi, J. Phys. Chem. B (Lett.) **113**, 2221 (2009).
- [55] S. Prestipino, F. Saija, and G. Malescio, J. Chem. Phys. **133**, 144504 (2010).
- [56] Yu. D. Fomin and V. N. Ryzhov, Phys. Lett. A **375** 2181 (2011).
- [57] Yu. D. Fomin and V.N. Ryzhov, Adv. Chem. Phys. (in press) (arXiv:1008.0939v1 (2010)).
- [58] P.G. Debenedetti, V.S. Raghavan, and S.S. Borick, J. Phys. Chem. **95**, 4540 (1991).
- [59] Daan Frenkel and Berend Smit, *Understanding molecular simulation (From Algorithms to Applications)*, 2nd Edition (Academic Press), 2002.
- [60] D. Frenkel and A. J. Ladd, J. Chem. Phys. **81**, 3188 (1984).
- [61] Ya. Rosenfeld, Phys. Rev. A, **15**, 2545 (1977).
- [62] Ya. Rosenfeld, J. Phys.: Condens. Matter **11**, 5415 (1999).
- [63] R. Sharma, S. N. Chakraborty, and Ch. Chakravarty J. Chem. Phys. **125**, 204501 (2006).
- [64] A. B. de Oliveira, E. A. Salcedo Torres, Ch. Chakravarty, M. C. Barbosa, arXiv:1002.3781 (2010).
- [65] Yu. D. Fomin, V. N. Ryzhov, and N. V. Gribova, Phys. Rev. E **81**,061201 (2010).
- [66] A. Samanta, Sk. Musharaf Ali, S. K. Ghosh, J. Chem. Phys. **123**, 084505 (2005).
- [67] J. J. Hoyt, Mark Asta, and Babak Sadigh, Phys. Rev. Lett. **85**, 594 (2000).
- [68] A. Samanta, Sk. Musharaf Ali, and S. K. Ghosh, Phys. Rev. Lett. **87**, 245901 (2001).
- [69] A. Samanta, Sk. Musharaf Ali, and S. K. Ghosh, Phys. Rev. Lett. **92**, 145901 (2004).
- [70] M. Agarwal, A. Ganguly, and Ch. Chakravarty J. Phys. Chem. B, **113**, 15284 (2009).
- [71] M. Agarwal and Ch. Chakravarty, Phys. Rev. E, **79**, 030202(R) (2009).
- [72] Zh. Yan, S. V. Buldyrev, and H. Eu. Stanley, Phys. Rev. E, **78**, 051201 (2008).
- [73] T. Goel, Ch. N. Patra, T. Mukherjee, and Ch. Chakravarty, J. Chem Phys. **129**, 164904 (2008).
- [74] W.P. Krekelberg, T. Kumar, J. Mittal, J.R. Errington and T.M. Truskett, Phys. Rev. E **79** 031203 (2009).
- [75] M. J. Pond, W. P. Krekelberg, V. K. Shen, J. R. Errington and Th. M. Truskett, J. Chem. Phys. **131**, 161101 (2009).
- [76] P.H. Poole, F. Sciortino, U. Essmann, and H.E. Stanley, Nature **360**, 324 (1992).
- [77] L. Xu, P. Kumar, S.V. Buldyrev, S.-H. Chen, P.H. Poole, F. Sciortino, and H.E. Stanley, PNAS **102**, 16558 (2005).
- [78] P. Kumar, S.V. Buldyrev, S.R. Becker, P.H. Poole, F.W. Starr, and H.E. Stanley, PNAS **104**, 9575 (2007).
- [79] G. Franzese and H. E. Stanley, J. Phys.: Condens. Matter **19**, 205126 (2007).